



Effect of powder heat treatment on fatigue mechanisms of freestanding AA7075 cold spray deposits



C.J. Williamson^a, A.R. Webb^a, L.N. Brewer^b, P.G. Allison^c, J.B. Jordon^{c,*}

^a Dept. of Mechanical Engineering, The University of Alabama, Tuscaloosa, AL 35487, USA

^b Dept. of Metallurgical and Materials Engineering, The University of Alabama, Tuscaloosa, AL 35487, USA

^c Dept. of Mechanical Engineering, Baylor University, Waco, TX 76798, USA

ARTICLE INFO

Keywords:

Cold Spray
Aluminum Alloys
Fatigue
Fractography
Powder Processing

ABSTRACT

In this work, the effect of powder heat treatment on the tensile and fatigue properties of freestanding cold sprayed specimens was characterized. Overaged and solutionized powder depositions demonstrated increased ductility but decreased yield strength compared to the as-atomized condition. The as-atomized and overaged specimen exhibited nearly identical fatigue behavior, while the solutionized powder specimen demonstrated increased fatigue performance. The improvement in cyclic performance is credited to the dissolution of intermetallics that were present in the as-atomized and overaged powder conditions that effectively reduce fatigue crack growth resistance.

1. Introduction

Cold spray is a solid-state deposition process that uses supersonic gas to accelerate powder to a critical velocity that causes the powder particles to plastically deform upon impact and to metallurgically bond with the substrate. The collision and subsequent bonding allows for the manufacturing of additive depositions and the repair of worn or damaged components [1]. Since cold spray is a low heat input process, there is minimal distortion to the substrate from thermal warping making it an attractive option for additive structural repair [2]. Increasingly, the use of cold spray as a method to repair and maintain aircraft has been established as a way to reduce downtime and the logistical strain of operation as worn or corroded parts have few current methods for restoration back to OEM specifications [3,4]. However, to reliably use cold spray for the repair of structural components, the mechanical properties of the deposits must be examined and characterized to support the maintenance and repair of the aircraft while maintaining the high level of safety and reliability required by industry.

Aluminum alloy 7075 is an Al-Zn-Mg-Cu alloy that sees extensive use in the aviation industry due to its high strength-to-weight ratio [5]. The aluminum alloy 7000 series derive their strength from precipitation hardening. Following a solution treatment, the alloys will precipitate out GP zones that coarsen and nucleate the metastable η' phase that exhibit coherency with the matrix and acts as the main hardening phase.

Longer exposures times at elevated temperatures can overage the η' phase into the incoherent η phase and resultingly decrease the strength of the alloy [6]. In addition, the formation of other phases and intermetallics such as the S-phase (Al-Mg-Cu rich), T-phase (Al-Zn rich), iron-rich intermetallics, and Mg₂Si have been seen to be the initiation sites for crack formation in fatigue loading of wrought plate that is a widely used material in aviation [7–10]. As aerospace components see regular cyclic loading, fatigue is a critical concern and has been addressed with several alloy modifications such as AA7050 and AA7475 that are differentiated by lower allowable amounts of iron and silicon content that limits the size and quantity of intermetallics and thus improves on fatigue performance [5].

The use of traditional fusion welding on AA7075 for structural repairs of damaged components is not considered a viable option as the alloy is generally considered unweldable due to its tendency to hot crack in the weld seam [11]. Other means of repair to increase the service life of components have been investigated with the use of composite patches implemented for mitigation of crack growth similar to the practice of using mechanically fastened metallic repairs. However, neither repair strategy allows for the return of the repaired component to OEM dimensions or the restoration of thinning and pitting due to corrosion damage [12,13]. The cold spray process has been demonstrated as a viable repair option for aluminium [14,15], magnesium [16,17], steel [18], and Inconel [19] alloys. Additionally, cold spray has been

* Corresponding author.

E-mail address: brian.jordon@baylor.edu (J.B. Jordon).

demonstrated to repair cracked panels [14] and damaged/worn bolt holes [15] that mimic the corrosion and mechanical damage that regularly occurs in the aerospace industry. In addition to merely returning the components to geometrical specifications, the repaired holes and grooves have been demonstrated to carry structural loads [20] and thus show feasibility of use in life extension programs.

While characterization of AA7075 cold spray has been widely reported in literature, only a few studies report on the effect of heat treatment on the pre-sprayed powder and post-deposition heat treatments. The effects of post-deposition heat treatment of cold sprayed AA7075 depositions has been studied by Rokini et al. [21] and shown that the heat treated materials exhibit nearly twice the ductility of the as-deposited specimen. Additionally, the effect of powder heat treatments [22–25] has been studied as a way to modify post-deposition properties without additional processing steps. Studies on powder heat treatments of AA7075 found that the condition of the powder prior to deposition has direct effects on deposition efficiency, porosity, and bonding strength. However, only limited mechanical testing has been performed to directly evaluate the potential for powder heat treatment on the mechanical properties of AA7075. Inert gas atomization is the standard method to prepare powders for use in cold spray, but metals prepared this way form dendritic microstructures with solutes such as the zinc forced out into intermetallic networks along cell boundaries. This network of intermetallics decreases the free solute in the particle for forming strengthening precipitates as well as creating a brittle network between cells that decreases the ductility of the particle during deposition. This resulting non-homogeneity in the particle subsequently leads to increased nonuniform plastic deformation upon deposition [26–28]. Heat treating the powder prior to spraying offers a path to improve the post-deposition microstructure and mechanical properties including fatigue.

Since fatigue resistance is a key performance metric for the usability of cold spray in repairing components for in-field use, several studies have been conducted to characterize the fatigue performance of cold spray [29]. As such, characterization studies of fatigue in cold sprayed materials generally focus on the application of coatings applied to a substrate or localized repairs on specimen to determine the effectiveness of the technique for repair [30–32]. These studies offer key insight into mechanisms controlling the usefulness of cold spray for repair, but the fatigue performance is often controlled by the interface of the deposition and the substrate that causes unique fracture and initiation mechanisms, such as compressive residual stresses in the substrate, but do not allow for an understanding of the inherent fatigue properties of the depositions themselves [32]. In a study by White et al. [33], freestanding specimens were prepared from as-atomized AA7075 and AA2024 powder in order to avoid the adhesion complications while evaluating the fatigue behavior of the cold sprayed material. In this work, White et al. reported a reduction in the number of cycles to failure when compared to wrought T6 specimen, where interlayer defects were found to be the cause of crack initiation. While their work examined the fatigue properties of freestanding cold spray in AA7075, the effect of various heat treatments of the powder prior to spraying was not evaluated. As such, in this present study, the effect of three heat treatments of the powder including, as-atomized, overaged, and solutionized, on fatigue mechanisms of freestanding cold spray materials is characterized for the first time.

2. Methods and materials

For this study, a VRC Gen III high pressure cold spray system was used to deposit the aluminum alloy 7075 deposits. Commercially off the shelf (COTS) as-atomized and overaged AA7075 powders were compared to solutionized powder. The solution treatment followed the procedures described elsewhere [23]. In this approach, as-atomized powder was heated in an inert gas-filled and rotating tube furnace to 480°C and held at temperature for 4 h to fully dissolve the

intermetallics. The solutionized powders were then stored below 0 °C until deposition to eliminate any natural aging of the powder. The deposition parameters were held constant for all three depositions and are presented in Table 1.

Fig. 1a displays the geometries for the monotonic and subscale fatigue specimens overlayed onto a representative cold spray deposition, while Fig. 1b and 1c are the nominal dimensions of the monotonic and subscale fatigue specimen respectively. Note, that the deposition was removed from the substrate prior to specimen machining to eliminate the possibility wrought material remaining in the mechanical test specimens. Subsequently, the specimen geometry was cut from the freed deposition using a wire electrical discharge machine (EDM) with the loading direction parallel to the raster direction of the deposition. After machining the specimens were then polished to a 600 grit finish parallel to the loading direction to remove stress concentrations and the recast layer from the wire EDM. For all mechanical testing, control specimens prepared from AA7075-T6 2.54 mm thick plate were prepared for comparison to the cold sprayed material and all tests were completed in triplicate to ensure repeatability. Mechanical testing was conducted with a 25 kN servohydraulic MTS landmark load frame in ambient laboratory atmosphere and temperature. The monotonic tests were performed with a 25.4 mm extensometer at a nominal strain rate of 0.001 mm/mm/s. The stress-controlled fatigue tests were conducted at 40Hz with a sine wave profile at a load ratio of $R = -1$. The stress amplitudes for the fatigue testing were chosen from between 30 % and 70 % of the wrought AA7075-T6 ultimate tensile strength (UTS).

Post-failure fractography of the fatigue specimens was conducted with an Apreo scanning electron microscope (SEM) at 5 keV with back scatter electron (BSE) detector and Everhart-Thornley detector (ETD). Metallographic specimens from the bulk depositions were prepared across the raster direction for each powder heat treatment and polished to 0.05 μm for use in measuring the porosity in the build using area fraction analysis in ImageJ from images taken with a Keyence 7000. These specimens were then etched with Keller's reagent and imaged with the Apreo SEM to examine the post-deposition microstructure as well as investigate the intermetallic network present in the powder particles in the different heat treatments.

3. Results

The SEM micrographs of the etched microstructures of the cold spray material are shown in Fig. 2 with the etchant highlighting the boundaries of the deformed powder particles referred to as prior particles once deposited. Fig. 2a and 2b display the as-atomized and overaged depositions, respectively, that exhibited evidence of preferential etching at the particle boundaries as well as etching of the zinc-rich intermetallic network on the face of the exposed particles, seen as the dark webbing across each particle. The etched microstructure of the solutionized deposition, seen in Fig. 2c, did not exhibit the etched intermetallic network and displayed significantly less etching at the particle boundaries suggesting a reduction in zinc-rich intermetallics present in the particles in both the bulk particle and the boundaries between the particles that results in a more homogenous microstructure.

The monotonic results of the cold spray powder heat treatments compared to the AA7075 control specimen are displayed in Fig. 3. All

Table 1
Cold Spray Parameters.

	AA7075-T6
Substrate	Helium
Carrier Gas	3.45 MPa
Pressure	450 °C
Temperature	8.2 g/min
Powder Feed Velocity	200 mm/s
Gun Velocity	15 mm
Stand-off Distance	150 mm
Nozzle Length	

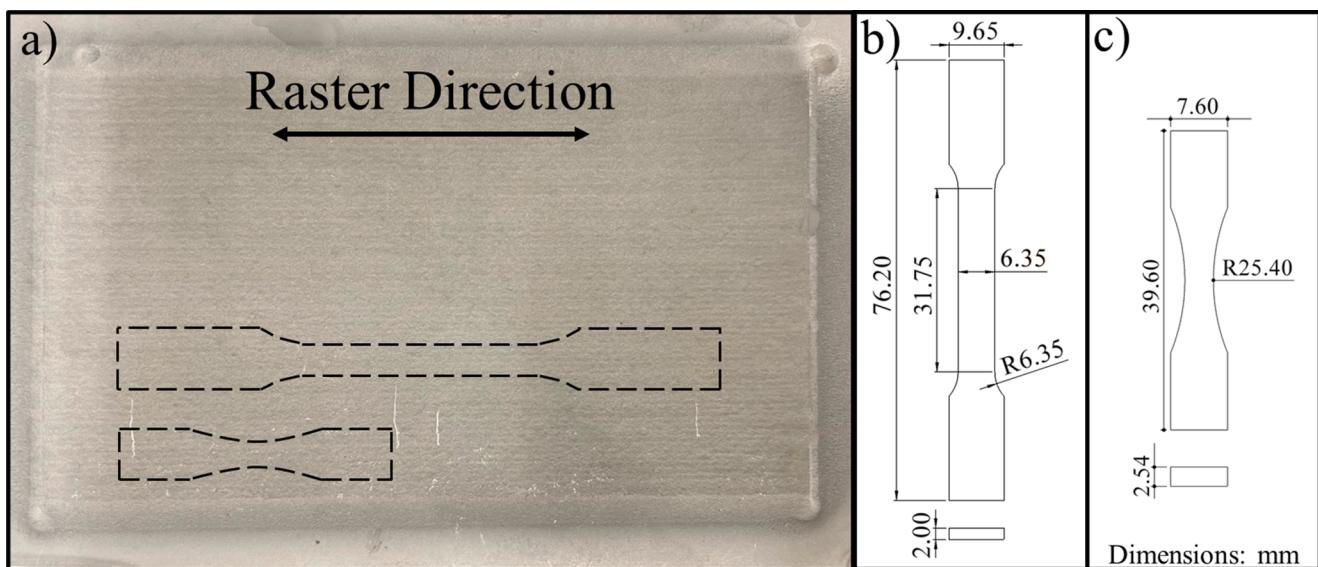


Fig. 1. (a) Representative bulk cold spray deposition with specimen oriented in direction of machining, (b) monotonic specimen geometry, and (c) fatigue specimen geometry.

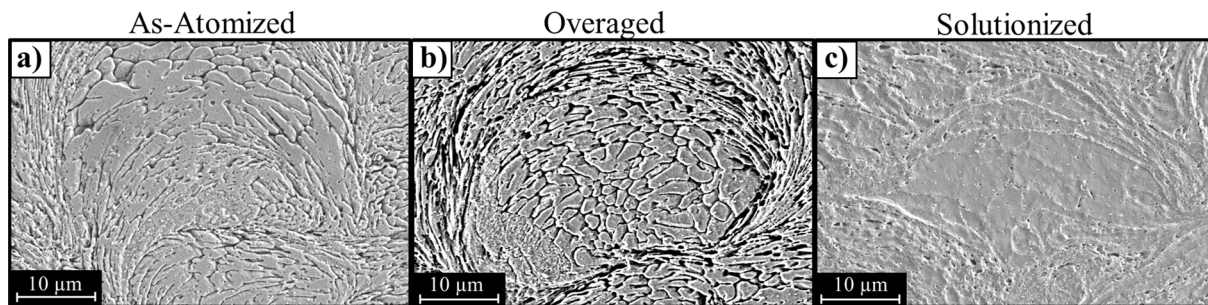


Fig. 2. SEM images of the etched microstructure of (a) as-atomized, (b) overaged, and (c) solutionized powder depositions displaying the etching of intermetallic networks throughout the particle and along particle boundaries of the overaged and as-atomized depositions.

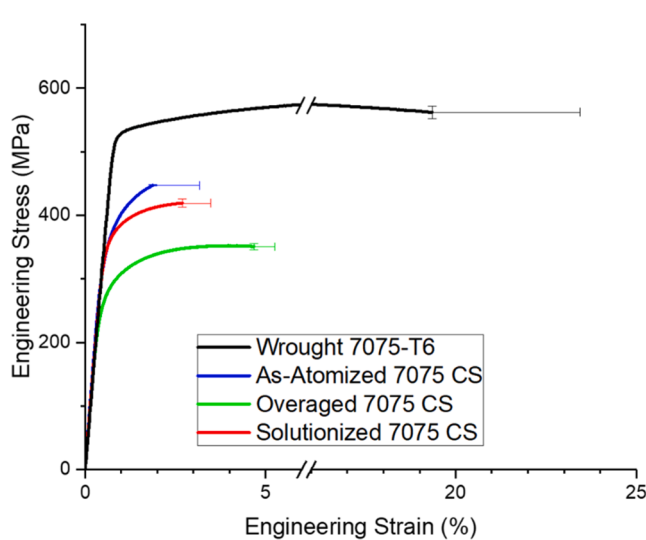


Fig. 3. Monotonic curves of the cold sprayed specimen with as-atomized, overaged, and solutionized powder compared to wrought T6 plate (Note the break in the x axis).

three cold spray curves displayed reductions in strength and ductility compared to the wrought T6 material but also demonstrated distinct tensile curve behavior due to the differences in particle microstructure. The as-atomized specimen exhibited the lowest strain to failure of the cold sprayed materials tested in this present study but had the highest ultimate tensile strength (UTS) and yield strength (YS). The overaged powder demonstrated a significant decrease in UTS of 89.1 MPa as compared to as-atomized treatment but had a 2 % increase in strain to failure that was nearly twice the elongation observed in the as-atomized powder. The solutionized powder deposition displayed an increase in strain to failure of 0.7 % compared to the as-atomized specimen, while only exhibiting a decrease in UTS of 37.2 MPa and having nearly

Table 2
Monotonic Mechanical Properties.

	Wrought 7075-T6	As- Atomized	Overaged	Solutionized
Yield (0.2 Pct Offset) (MPa)	531.5 ± 1.1	372.5 ± 1.9	278.3 ± 3.2	367.4 ± 1.1
Ultimate Tensile Strength (MPa)	583.4 ± 0.8	457.2 ± 10.3	368.1 ± 4.2	420.0 ± 4.8
Young's Modulus (GPa)	67.6 ± 1.1	71.9 ± 0.8	68.7 ± 1.0	68.9 ± 0.5
Elongation to Failure (pct)	21.9 ± 1.8	2.5 ± 0.7	5.1 ± 0.2	3.2 ± 0.3
Porosity (pct)		0.92 ± 0.25	0.21 ± 0.08	0.45 ± 0.12

identical YS properties. The error bars in Fig. 3 illustrates the variation in the strain-to-failure between the maximum and minimum fracture strain for each material. Additionally, the summary of the mechanical properties is displayed in Table 2. Also reported in Table 2 are the corresponding porosity measurements of the three depositions illustrating that all depositions exhibited a < 1 % porosity.

The fatigue S–N curves of the freestanding cold spray with the three powder heat treatments compared to the AA7075-T6 control specimen are shown in Fig. 4a. Interestingly, across all stress amplitudes tested, the overaged and as-atomized powder displayed nearly identical cycles to failure despite the differences in the elongation to failure and UTS. Contrarily, the solutionized powder deposition that demonstrated monotonic properties similar to the as-atomized powder exhibited a marked increase in number of cycles to failure over the other powder heat treatments with an order of magnitude increase in the average number of cycles to failure at the highest and lowest stress amplitudes tested. Even so, the solutionized powder deposition still resulted in a reduction of fatigue life compared to the control. Additionally, the solutionized deposition exhibited an increase in the runout stress at 10^7 cycles compared to the other cold spray depositions demonstrating an increase in the fatigue threshold. Fig. 4b is an S–N curve with the applied stress normalized by the ultimate tensile strength of each material. When normalized, the solutionized and overaged particle depositions exhibited similar performance. Normalization of the fatigue results in this present study demonstrates that there is no correlation to tensile strength for the heat treated cold sprayed materials.

Fig. 5a depicts representative fractography of the three regions observed on the cold sprayed fracture surfaces for an overaged powder specimen subjected to fatigue loading. In the small crack regime near the crack initiation point, there was preferential transparticle (through prior particle) growth observed that left a smooth and flattened surface as seen in Fig. 5b. As the crack grew, the stress intensity increased and thus caused a change in the dominant fracture mechanism. From Fig. 5c it is clear that interparticle crack growth along the particle boundaries began to occur as seen by the smooth, rounded marks, highlighted by red arrows, likely due to the increased driving force allowing for nonplanar crack growth. This dual mechanism region displays both particle boundary cleavage and transparticle crack growth. The ratio of these two fracture mechanisms is likely controlled by the stress intensity seen at that crack length as well as the orientation of the particle boundaries in relation to the plane of maximum tensile shear. The proportion of interparticle fracture compared to transparticle on the fracture surface

increased with crack length until fast fracture occurred (Fig. 5d), where the remaining material could not support the applied load and rupture occurred.

Representative post-mortem fractography of the crack initiation sites can be seen in Fig. 6. For each of the powder heat treatments, the depositions exhibited near surface initiation from porosity and lack of complete particle bonding. Fig. 6a and 6b both display crack initiation from a lack of metallurgical bonding between particles causing fracture along the prior-particle boundary before entering the bulk material with the network of zinc rich intermetallics on the overaged particle surface seen in Fig. 6b. A representative crack initiation from near-surface porosity in a solutionized powder specimen can be seen in Fig. 6c, though initiation from porosity was observed for all three powder heat treatments. Further, each type of powder heat treatment depositions exhibited crack initiation from defects in the deposition rather than material discontinuities such as the iron-rich intermetallics that are often observed to cause crack initiation in wrought AA7075 [34]. Measurements of multiple crack initiation sites revealed an average $\sqrt{\text{area}}$ of $28.7 \pm 20.0 \mu\text{m}$ for the as-atomized, $29.3 \pm 19.9 \mu\text{m}$ for the overaged, and $30.1 \pm 18.5 \mu\text{m}$ for the solutionized specimens which is similar in scale to the size of powder particles with no definite shape or size difference of the initiation site being linked to a particular powder heat treatment. The variance in the $\sqrt{\text{area}}$ for any given powder largely dominates any defect size differences between the three powder conditions. Contrarily, the differences in defect size for a given powder condition, as seen qualitatively in Fig. 4a, does not lead to significant variation in the fatigue life with each specimen type exhibiting less variability than the wrought counterpart.

At the same nominal stress amplitude of 173 MPa, there was a difference observed in the size of the transparticle growth region that can be seen in the highlighted region of Fig. 7 when comparing the as-atomized and overaged specimen (Fig. 7a and 7b) with the solutionized powder (Fig. 7c). Noticeably, the solutionized powder specimen demonstrated an increase in size of the region of transparticle growth around the crack initiation point as well as displaying increased homogeneous crack growth in the near-initiation fracture surface (Fig. 7f). Additionally, both the as-atomized (Fig. 7d) and the solutionized specimens (Fig. 7e) exhibited some deviations but are largely contained to a flat plane of crack growth in the small crack regime that is perpendicular to the loading direction. Whereas the transparticle region of the overaged specimen, Fig. 7e, displayed evidence of preferential crack growth and particle deformation observed by the nonplanar crack

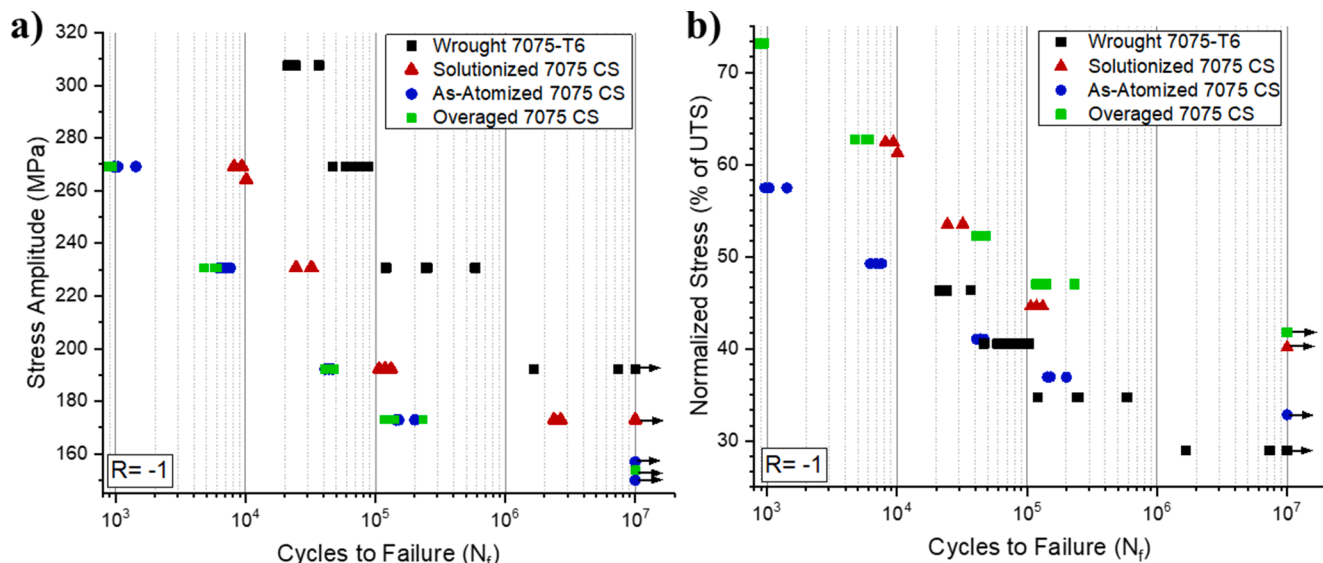


Fig. 4. (a) S–N curve comparing the as-atomized, overaged, and solutionized powder depositions with a wrought T6 curve for comparison. (b) S–N curve that has been normalized by the ultimate stress for each materials showing that the overaged powder has the greatest relative performance compared to the other materials.

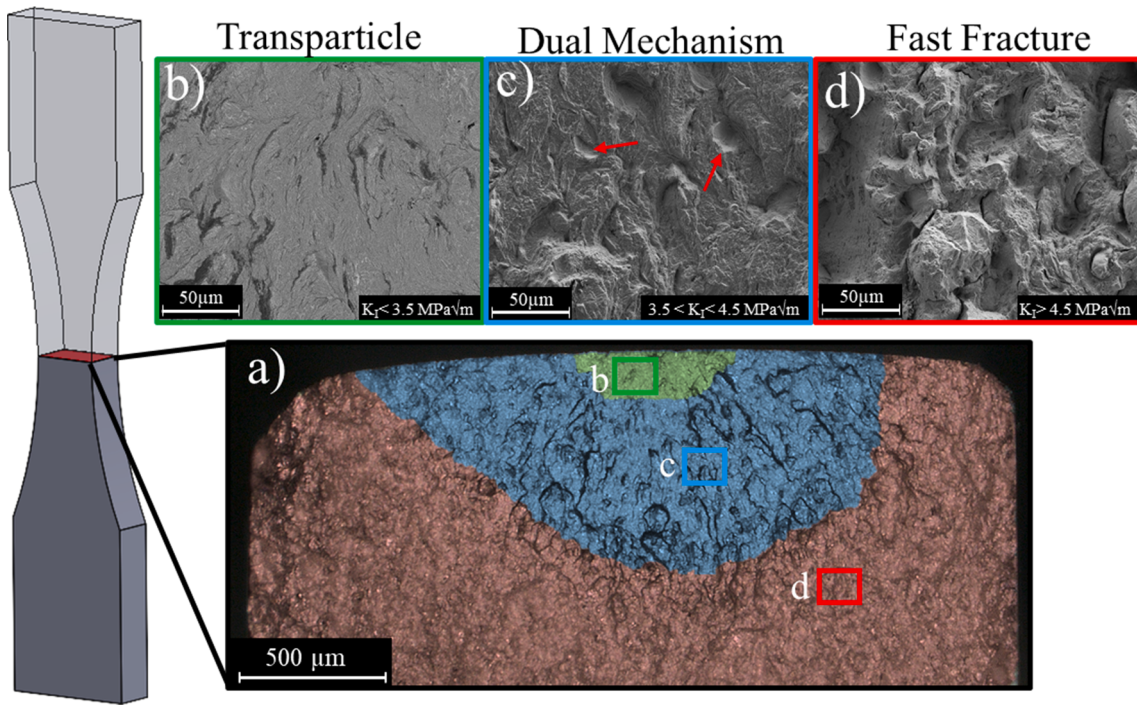


Fig. 5. (a) Partial portion of OM fractography of an overaged HCF specimen highlighting the three regions of crack growth with representative SEM fractography from (b) transparticle small crack growth regime, (c) dual mechanism regime, and (d) fast fracture regime.

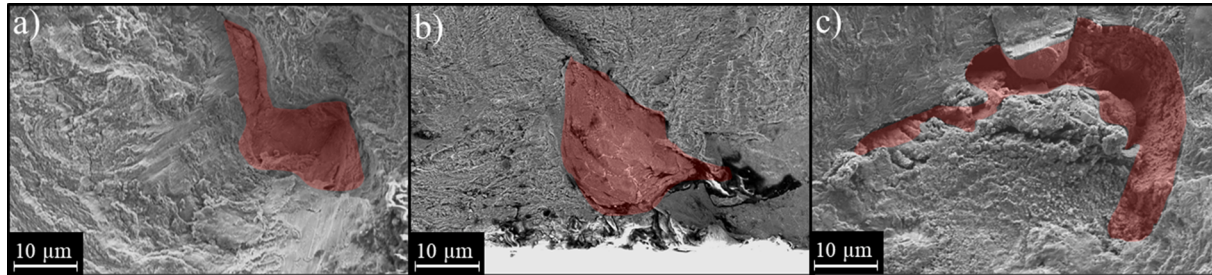


Fig. 6. SEM micrographs of the general types of crack initiation sites of all cold sprayed powder heat treatments (a) powder particle fracture, (b) lack of bonding between powder particles, and (c) porosity (Red overlays indicate approximate location and extent of crack initiation site for each micrograph).

growth. Fig. 7g-i display the dual fracture mechanism regime away from the crack initiation site. The three powder heat treatments all demonstrated fracture along particles boundaries due to interparticle fracturing with small areas of transparticle growth present. As such, the powder heat treatment did not exhibit significant differences in fracture mechanisms between individual heat treatments once the crack growth entered the transparticle regime.

Calculation of the stress intensity needed to transfer between the transparticle and dual mechanism regimes was accomplished using a simple linear elastic relationship (Eqs. (1)–(3)) for a small semi-elliptical crack [35].

$$K_I = \frac{1.12 * \sigma \sqrt{\pi a}}{\Psi} * g(\phi) \quad (1)$$

$$\Psi = \frac{3\pi}{8} + \frac{\pi}{8} \frac{a^2}{c^2} \quad (2)$$

$$g(\phi) = [\sin^2 \phi + \frac{a^2}{c^2} \cos^2 \phi]^{\frac{1}{2}} \quad (3)$$

In Eq. (1), K_I is the mode one stress intensity generated from the nominal stress σ and is a function of the length of the crack, a . A geometrical term Ψ (Eq. (2)) relates the stress intensity as a function of

the ratio of the long and short axes of the ellipse to account for effects of the crack growth aspect ratio. Eq. (3) is a term $g(\phi)$ that modifies the stress intensity as a function of angle across the semi-elliptical crack extension. Crack length measurements using the ImageJ software of SEM micrographs allowed for calculation of the stress intensity values displayed in Table 3. Crack length measurement demonstrated fluctuations in the critical stress intensity that varied randomly across the angle ϕ rather than uniformly leading to an increased scatter in the stress intensity measurement. This trend can be seen qualitatively in Fig. 7 (a-c) as the highlighted regions show deviancy from an ellipse. The inconsistent border between the transparticle and dual mechanism regions is likely controlled by variables such as prior-particle boundary orientation as well as the ability to achieve the critical stress intensity while still entrapped in a prior-particle thereby effectively extending the transparticle region along that angle.

Higher magnification SEM image comparison between the solutionized and overaged transparticle region is shown in Fig. 8. The solutionized powder deposition, Fig. 8a and b, demonstrates the presence of isolated intermetallics on the fracture surface seen as white particles. The difference between the transparticle and later crack growth stages can be seen by the relative uniformity in the transparticle region with significant crack deflection becoming increasingly common

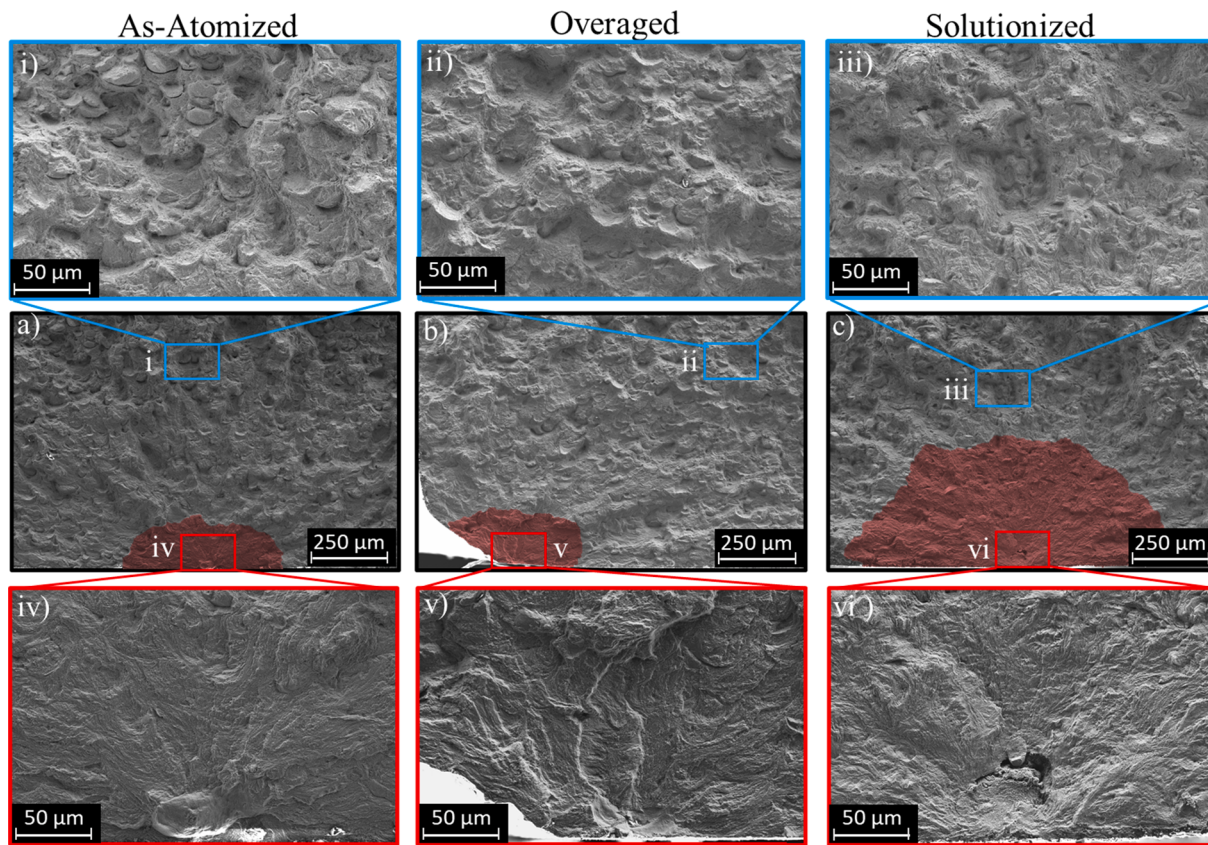


Fig. 7. SEM fractography of each powder condition, (a) as-atomized ($N_f = 150780$), (b) overaged ($N_f = 1518028$), and (c) solutionized ($N_f = 3662509$); tested at the same stress amplitude (173 MPa) with the region of transparticle growth highlighted in red. Higher magnification images of the transparticle growth regions (i-iii) of each specimen focused at the crack initiation point displaying the difference in transparticle growth between the heat treatments with images of the dual mechanism region (iv-vi) displaying little difference in this crack growth regime between the three powder heat treatments.

Table 3
Transparticle stress intensity distribution.

Powder Heat Treatment	Stress Intensity (MPa \sqrt{m})
As-Atomized	3.06 ± 0.36
Overaged	3.53 ± 0.18
Solutionized	4.05 ± 0.39

as the driving force for crack growth increases. When examining the overaged powder deposition, Fig. 8c and d, the intermetallic network that was seen in the etched particle is shown to be present all over the fracture surface in both the transparticle and dual mechanism images, as pointed out in the higher magnification images in Fig. 8e-f with red arrows.

Representative areas of fast fracture present in specimens tested at 192 MPa amplitude are shown in Fig. 9 with each powder condition exhibiting mixed ratios of ductile and brittle failure. The as-atomized and solutionized specimens (Fig. 9d and f) exhibited smooth regions of cleavage through particles as well as debonding along particle boundaries. Representative fractography images of the overaged powder specimen (Fig. 9b) demonstrated that the fast fracture regime was also dominated by particle separation as seen by the significant presence of rounded particle surfaces. However, the particle boundaries exposed did not exhibit the same smooth prior particle shape that was present on other two heat powder heat treatments. The smeared and dull appearance as well as the lack of the smooth regions of fractured particle boundaries across the fracture surfaces indicates an increased amount of ductility that correlates with the increased ductility seen in the monotonic testing. All three powder heat treatment types exhibited areas of

micro-void coalescence, but the failure mechanism is dominated by areas of particle boundary debonding with the ductile rupture of the surrounding material due to the void created by the particle debonding acting as a stress concentrator.

Examination of the low cycle fatigue fracture surfaces, as shown in Fig. 10, demonstrates that the higher stress amplitude reduces or potentially eliminates certain crack growth regimes. In Fig. 10a and b, the fracture surfaces of the as-atomized and overaged powder specimen do not display regions of solely transparticle fracture at this high stress amplitude. The solutionized specimen does exhibit a small region of transparticle fracturing but reduced from the size seen in the HCF fracture surface.

4. Discussion

4.1. Monotonic properties

The experimental monotonic results demonstrate that the microstructure of the AA7075 powder prior to deposition has distinct effects on the post-deposition properties. The solutionized and overaged powders demonstrated an increase in elongation to failure compared to the as-atomized powder while deleteriously affecting the yield strength. Cold sprayed material exhibits lower ductility compared to the wrought material in numerous alloys due to the cold sprayed material being limited by the particle-to-particle bonding as well as the effect of work hardening of the powder particle due to the extensive plastic deformation during impact. Examination of the fast fracture regime in Fig. 9d-f illustrated the difference in ductility of the powders as the as-atomized and solutionized specimen exhibit areas of smooth debonding particle boundaries as well as cleaved particles with minimal deformation, while

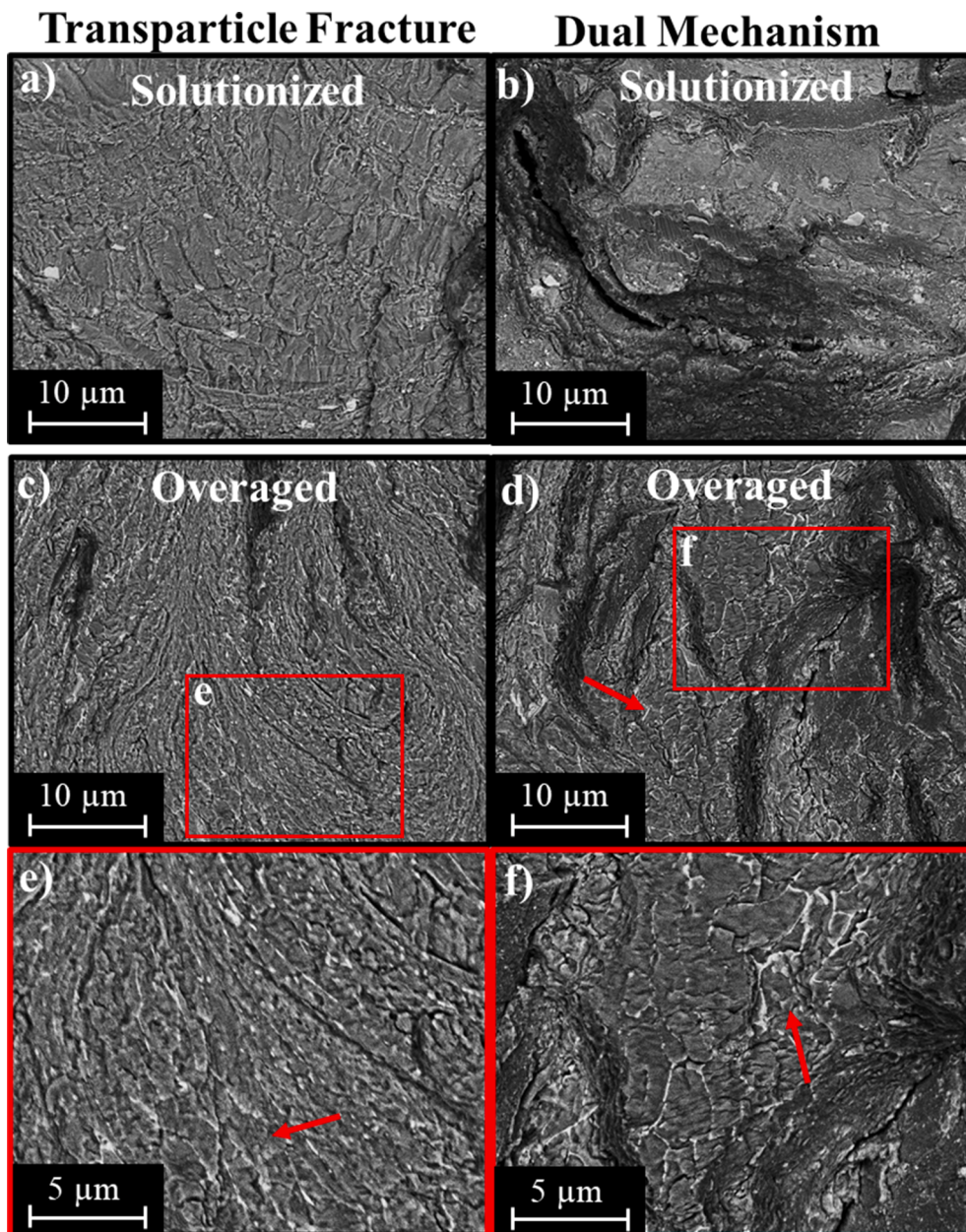


Fig. 8. SEM fractography demonstrating the difference between the transparticle and dual mechanism region for the (a-b) solutionized powder deposition and (c-d) overaged powder deposition. (e-f) are higher magnification images of the intermetallic network found on the fracture surface of the overaged powder deposition.

the overaged powder specimen revealed increased particle deformation. Resultingly, the solutionized and as-atomized depositions accommodated less plastic deformation than the overaged specimens as demonstrated by the monotonic properties. Conversely, the lack of particle deformation demonstrates the as-atomized and solutionized powder exhibit increased resistance to deformation resulting in overload failure due to the rupture of prior particle interfaces leading to increased strength but limited ability to accommodate plastic strain. Powder heat treatment of aluminum alloys in previous studies have demonstrated similar microstructural and spray behavior changes with heat treatment including hardness, precipitation development, and deposition efficiency [23,28]. Sabard et al. [22] reported similar fracture changes in a study on the effect of powder heat treatment on porosity, particle deformation, and bonding, where the solution treated AA7075 powder failed along particle boundaries in a monotonic test while heat treating the powder to T6 demonstrated a change to fracturing through the particle.

4.2. Fatigue performance and fracture regimes

The solutionized specimen exhibited an increase in the fatigue life across all fatigue stress levels that can likely be attributed to the elimination of intermetallic networks as demonstrated in Fig. 8. Crack nucleation and growth through the microstructure is detrimentally affected by the presence of a network of intermetallics in and surrounding the aluminum matrix. Similar observations have been found in work by Gavras et al. [36] on the crack growth rates of heat treated AA6061 cold spray depositions that documented that the annealed and as-sprayed specimen demonstrated a lower stress intensity threshold than specimens solutionized and heat treated to a T6 condition. While the smaller, transparticle crack growth regime in the current study could likely reduce the cycles to failure due to an earlier activation of an additional fracture mechanism, it would not be solely responsible for the increase in life or fatigue threshold observed in the solutionized specimen as the majority of the life of the high cycle fatigue specimen is

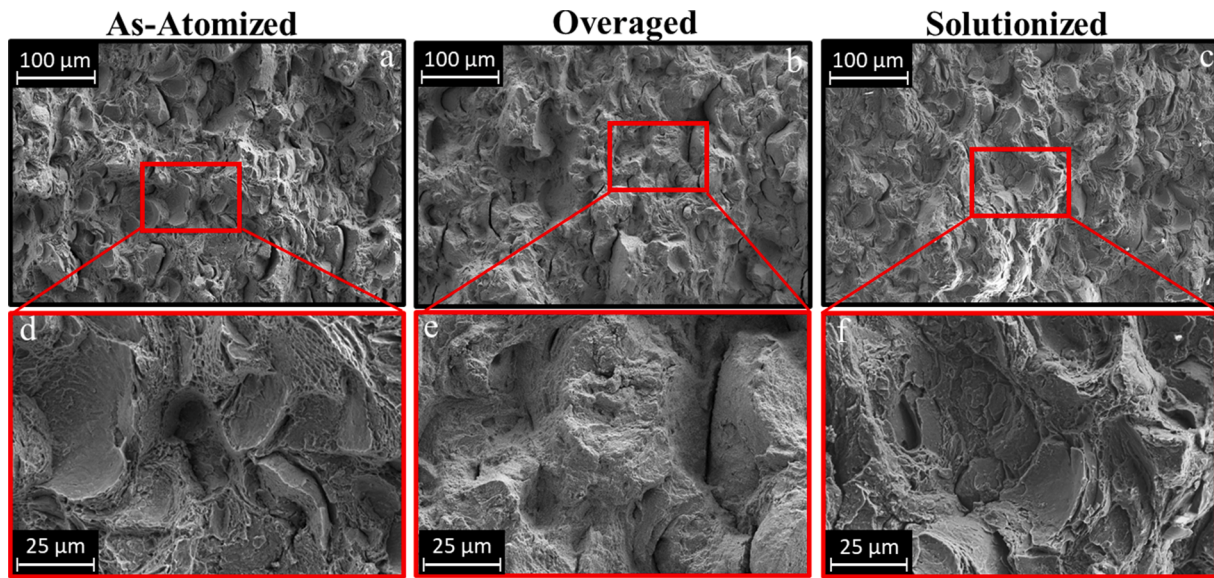


Fig. 9. SEM fractography of representative regions of fast fracture of (a) as-atomized, (b) overaged, and (c) solutionized powder with (d-f) higher magnification displaying signs of particle cleavage in the as-atomized deposition and particle debonding in the solutionized and as-atomized depositions.

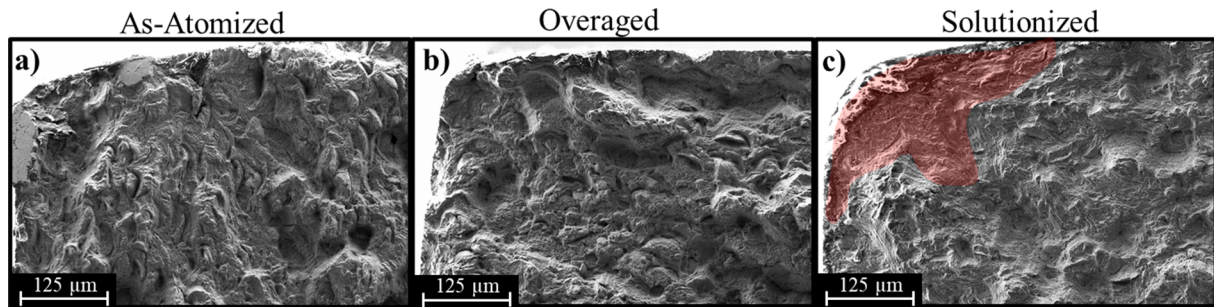


Fig. 10. SEM fractography of each powder heat treatment specimen in the low cycle fatigue regime at the same nominal stress amplitude (230 MPa). The (a) as-atomized ($N_f = 6928$) and (b) overaged ($N_f = 5824$) specimen demonstrated a lack of pure transparticle crack growth region. The (c) solutionized specimen ($N_f = 32242$) retains a small area of transparticle growth but reduced compared to the lower stress amplitude specimen.

spent nucleating a crack. Similarly, crack initiation sites were found to be unaffected by the powder heat treatment occurring solely from bonding defects and would thereby would not likely control the increase in cyclic performance. However, the overaged and as-atomized powder exhibited similar etched boundaries and intermetallic network that would suggest the reason for the nearly identical fatigue life of the two powders is the intermetallic networks alloy decreases the damage needed to initiate a crack.

All three heat treated powders demonstrated crack initiation from similar defects in both size, shape and mechanism that would not account for the significant difference in the fatigue life of the solutionized specimen. As areas of porosity and poor bonding can be problematic in the cold spray process due to nonuniform deformation of individual particles, the initial stress concentration appears nearly independent of the powder heat treatment and so would not account for the increase in life seen in the solutionized deposition [27,37]. In a study by Sabard et al. on the effects of powder heat treatments in the deformation of particle powders, the solutionized powder exhibited significant plastic deformation that induced cracking at the edges of the particle, while the peak aged powder caused material jetting from the substrate material. As such, the complex deformation mechanisms during particle and substrate bonding were observed to lead to porosity inside the cold sprayed depositions [38]. The similitude of initiation mechanism from bonding defects demonstrates that the solutionized deposition exhibited an increased resistance to crack growth as seen by an increase in life of

the specimens shown in Fig. 4 and in particular by the increase in fatigue threshold where no measurable crack had developed. The differences in fatigue life in a group of specimens at a nominal stress amplitude are controlled by differences in the microstructure of the specimen as well as defect size and position as slight variances in intermetallics, porosity size, or local development of slip bands can significantly affect the number of cycles to failure of a specimen [39,40]. The consistency of the fatigue lives across the limited specimen number tested in this present study for each specimen compounded with the similarity in initiation sites shown in Fig. 6 demonstrates that similar mechanisms control the crack initiation sites without significant deviance resulting from the powder heat treatments.

Fractographic examination of the small crack growth regime established that the powder microstructure controlled the fracture behavior by the detrimental presence of the brittle second phase network found in the non-solutionized specimen. Fig. 7e illustrated that the microstructure of the overaged particles was affecting crack propagation likely due to the nonuniformity of the particle microstructure from the formation of intermetallic networks as well as increased deformation due to the weaker overaged particles. The solutionized specimen fracture surface (Fig. 7f) displayed increased homogeneity in the transparticle crack growth region as compared to the overaged specimen that was tested at the same stress amplitude with the crack path leaving a smooth surface that results from solution treatment of the particles. Story et al. [23] observed that solution treating the powder reduces the amount of

intermetallics seen in the deposition and that as-atomized powders with the intermetallic networks present retain their intermetallic structures post deposition. Higher magnification examination of the transparticle and dual mechanism of the overaged powder specimen, as shown in Fig. 8e-f, demonstrated that the intermetallic network was present on the fracture surface in both regions indicating that they contribute crack growth either by fracturing ahead of the crack tip or by offering preferential sites of fracture. As the intermetallics represent network of incoherently bonded interfaces within the aluminum matrix, the mismatch in properties such as modulus of elasticity and yield strength create stress concentrations that result in damage accumulation through separation or rupture of the intermetallic and the aluminum matrix initiating a crack and reducing the nucleation life. Similar observations in wrought material have been demonstrated with the overaged microstructure in wrought AA7075-T7351 exhibiting inferior fatigue life as compared to underaged and peak aged (T651) microstructure in AA7075 plate where the threshold value, the stress intensity needed to propagate the crack, was seen to be deleteriously effected by the overaged heat treatment [38,41]. In work by Suresh et al. [38] the difference in threshold value was suggested to be due to the interplay between environmental effects with a change in slip mechanism near the crack tip with the peak aged and underaged microstructures exhibiting slip bands shearing through the strengthening precipitates, while the over aged specimen displayed signs of dislocation looping due to the coarsened microstructure. As the crack grows, all three powder heat treatments displayed similar fracture surfaces in the dual mechanism region because the stress intensity ahead of the crack tip is likely enough to overcome small microstructural inhomogeneities in the particles with only particle-to-particle boundaries offering large enough discontinuities to cause crack deflection. This change in crack growth response has been established in wrought materials where the controlling mechanism behind crack propagation changes is based on the crack length between microstructurally small cracks, physically small crack, and long cracks [42].

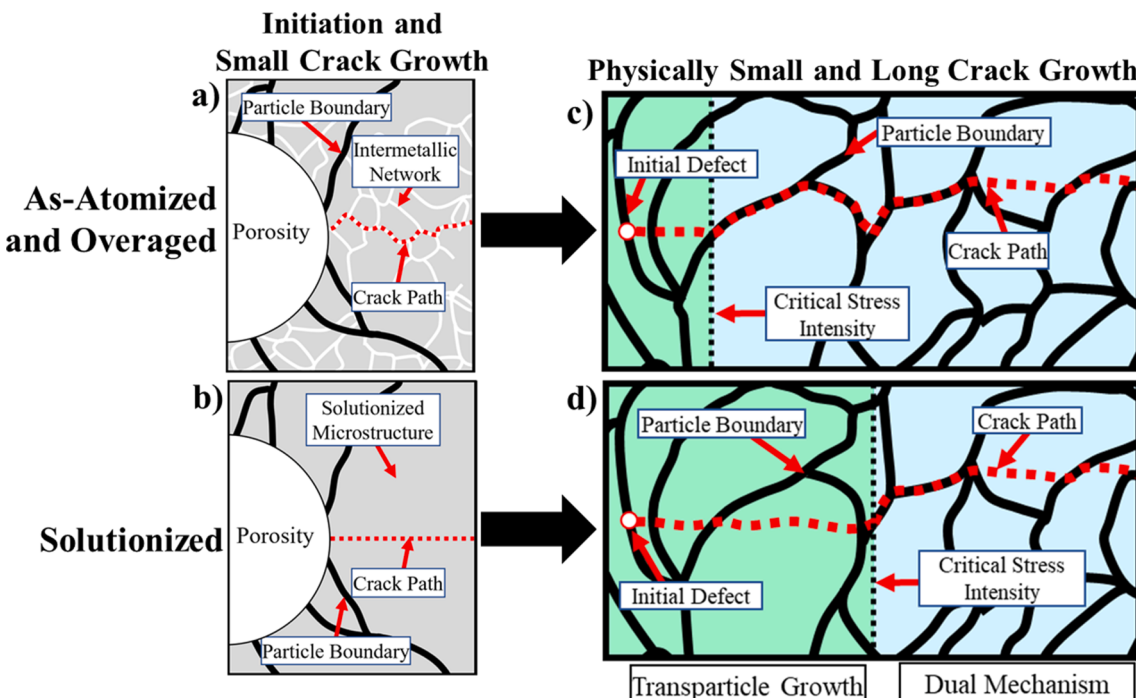


Fig. 11. Depiction of the influence of an intermetallic network on the microscale initiation and small crack growth regimes of the as-atomized/overaged (a) and the solutionized (b) powder deposition with (c-d) demonstrating macroscopically the difference that would be observed by a reduction in stress intensity needed to change the fracture mechanisms controlling long crack growth behavior.

4.3. Intermetallic network effect on early fatigue crack growth

Fig. 11 illustrates the difference in the fatigue mechanisms between the solutionized powder, intermetallic-rich overaged, and as-atomized powder deposition. Fig. 11a and b depict the nucleation and mechanically small crack growth regime, where intermetallic networks are of comparable size to the crack. As generalized defects, the brittle intermetallics can easily reduce the stress needed to initiate a crack by fracturing in the plastic zone upon loading. After initiation, the crack can propagate either along the intermetallic network or between areas of intermetallic fracture. As the crack increases in length, Fig. 11c and d, the intermetallic network ceases to control the mechanism for crack growth but instead deleteriously affects the crack growth rates and ease of particle boundary fracture. The resulting fracture surface would look nearly identical between the two types of microstructures except for a smaller region of transparticle growth and the presence of the intermetallic network on the fracture surface, which have both been demonstrated in this present work. This proposed explanation also establishes why not only does the solutionized powder specimen have a higher fatigue life but also a higher fatigue threshold value as the stress amplitude needed to initiate and grow a crack outside of the plastic zone of the defect would be higher in a material without a defect network.

In this present study, the cold spray depositions were found to change fracture characteristics as a function of the crack length due to the stress intensity increasing. Similarly, this change in fracture mechanism has also been observed by Gavras et al. [31,36] in quantifying the long crack growth rates of cold sprayed AA6061, in which a change in the mechanism was observed to be linked to an increase in the crack growth rate with the transition controlled by the prior particle boundaries. Additionally, the study by Gavras et al observed this change in mechanism in an as-sprayed and artificially aged (344 °C, 8 h) depositions but not in depositions that were heat treated to a T6 condition, which exhibited a linear Paris like crack growth region similar to wrought material.

5. Conclusions

For the first time, aluminum cold sprayed depositions made from different powder heat treatments were mechanically tested to evaluate their stress-life fatigue properties and to elucidate the effect that the feedstock particle microstructure has on the potential for use in repair applications. Cold sprayed AA7075 exhibited promising mechanical results as the effects of two heat treatment conditions were compared to the as-atomized powder deposition. The overaged specimen displayed a higher ductility but also a reduction in yield strength and nearly identical fatigue life as the as-atomized specimens. Additionally, depositions made with fully solution treated powder exhibited a slight increase in elongation to failure and nearly identical yield strength as the as-atomized specimen, but also resulted in a considerable increase in fatigue life. Fractography revealed that all three types of depositions exhibited fatigue crack initiation from near-surface bonding defects and also revealed distinct fracture mechanisms as the crack grew. The fatigue cracks were observed to propagate through particles in the small crack regimes leaving behind a flat fracture surface before preferentially fracturing along prior particle boundaries prior to rupturing via a mixture of particle cleavage and debonding as well as microvoid coalescence in the fast fracture region. The monotonic properties were observed to be directly related to the fracture mechanisms in the fast fracture region where the as-atomized and solution treated specimens displayed areas of brittle fracture mechanism while in contrast the overaged specimen demonstrated increased particle deformation. The increase in number of cycles to failure observed in the solutionized powder is a strong indicator in the potential to further improve deposition properties of cold spray in pursuit of structural component repair.

Declaration of Competing Interest

The authors declare the following financial interests/personal relationships which may be considered as potential competing interests: Dr. Luke Brewer reports financial support was provided by Office of Naval Research.

Data availability

Data will be made available on request.

Acknowledgment

The authors are very grateful for funding for this research from Mr. Bill Nickerson, Dr. Anisur Rahman, and Dr. Jennifer Wolk at the Office of Naval Research under grants N00014-15-1-2133 and N00014-18-1-2519.

References

- [1] Lee JC, Kang HJ, Chu WS, Ahn SH. Repair of Damaged Mold Surface by Cold-Spray Method. *CIRP Ann* 2007;56(1):577–80.
- [2] Champagne V, Helfritch D. Materials Science and Technology Critical Assessment 11: Structural repairs by cold spray Critical Assessment 11: Structural repairs by cold spray, 2014. 10.1179/1743284714Y.0000000723.
- [3] Jones R, Matthews N, Peng D, Singh Raman RK, Phan N. Experimental studies into the analysis required for the durability assessment of 7075 and 6061 cold spray repairs to military aircraft. *Aerospace* 2020;7:119. <https://doi.org/10.3390/AEROSPACE7090119>.
- [4] Leyman PF, Champagne VK. Cold Spray Process Development for the Reclamation of the Apache Helicopter Mast Support, 2009.
- [5] Dursun T, Soutis C. Recent developments in advanced aircraft aluminium alloys. *Mater. Des.* 2014;56:862–71. <https://doi.org/10.1016/j.matdes.2013.12.002>.
- [6] Banhart J. Age hardening of aluminum alloy. *Bull Alloy Phase Diagrams* 1984;5:21. <https://doi.org/10.1007/BF02868712>.
- [7] Weiland H, Nardiello J, Zaefferer S, Cheong S, Papazian J, Raabe D. Microstructural aspects of crack nucleation during cyclic loading of AA7075-T651. *Eng Fract Mech* 2009;76(5):709–14.
- [8] Li P, Marchand NJ, Ilschner B. Crack initiation mechanisms in low cycle fatigue of aluminium alloy 7075 T6. *Mater Sci Eng A* 1989;119:41–50. [https://doi.org/10.1016/0921-5093\(89\)90522-4](https://doi.org/10.1016/0921-5093(89)90522-4).
- [9] Jordon JB, Horstemeyer MF, Solanki K, Bernard JD, Berry JT, Williams TN. Damage characterization and modeling of a 7075-T651 aluminum plate. *Mater Sci Eng A* 2009;527(1-2):169–78.
- [10] Gupta VK, Agnew SR. Fatigue crack surface crystallography near crack initiating particle clusters in precipitation hardened legacy and modern Al-Zn-Mg-Cu alloys. *Int J Fatigue* 2011;33(9):1159–74.
- [11] Çevik B. Gas tungsten arc welding of 7075 aluminum alloy: microstructure properties, impact strength, and weld defects. *Mater Res Express* 2018;5:066540. <https://doi.org/10.1088/2053-1591/AACBCB>.
- [12] Albedah A, Khan SMA, Benyahia F, Bachir Bouiadra B. Experimental analysis of the fatigue life of repaired cracked plate in aluminum alloy 7075 with bonded composite patch. *Eng Fract Mech* 2015;145:210–20. <https://doi.org/10.1016/J.ENGFRACMECH.2015.04.008>.
- [13] Ratwani MM. Repair Options for Airframes, (n.d.).
- [14] Cavaliere P, Silvello A. Crack Repair in Aerospace Aluminum Alloy Panels by Cold Spray. *J Therm Spray Technol* 2017;26(4):661–70.
- [15] White B, Story W, Brewer L, Jordon JB, Brian J. Fatigue behaviour of fastener holes in high-strength aluminium plates repaired by cold spray deposition. *Fatigue Fract Eng Mater Struct* 2020;43:317–29. <https://doi.org/10.1111/ffe.13144>.
- [16] Champagne VK. The repair of magnesium rotorcraft components by cold spray. *J Fail Anal Prev* 2008;8(2):164–75. <https://doi.org/10.1007/s11668-008-9116-y>.
- [17] V.C. Jr, Kaplowitz D, V.K.C. III, Howe C, West MK, McNally B, Rokni M. Dissimilar metal joining and structural repair of ZE41A-T5 cast magnesium by the cold spray (CS) process, 10.1080/10426914.2016.1257137. 33 (2017) 130–139. 10.1080/10426914.2016.1257137.
- [18] Faccoli M, Cornacchia G, Maestrini D, Marconi GP, Roberti R. Cold Spray Repair of Martensitic Stainless Steel Components, (n.d.). 10.1007/s11666-014-0129-7.
- [19] Ogawa K, Seo D. Repair of Turbine Blades Using Cold Spray Technique, (n.d.). 10.5772/23623.
- [20] Petrácková K, Kondás J, Guagliano M. Fixing a hole (with cold spray). *Int J Fatigue* 2018;110:144–52. <https://doi.org/10.1016/j.ijfatigue.2018.01.014>.
- [21] Rokni MR, Widener CA, Champagne VK, Crawford GA, Nutt SR. The effects of heat treatment on 7075 Al cold spray deposits. *Surf Coatings Technol* 2017;310:278–85. <https://doi.org/10.1016/j.surfcoat.2016.10.064>.
- [22] Sabard A, McNutt P, Begg H, Hussain T. Cold spray deposition of solution heat treated, artificially aged and naturally aged Al 7075 powder. *Surf Coatings Technol* 2020;385:125367. <https://doi.org/10.1016/j.surfcoat.2020.125367>.
- [23] Story WA, Brewer LN. Heat Treatment of Gas-Atomized Powders for Cold Spray Deposition. *Metall Mater Trans A Phys Metall Mater Sci* 2018;49(2):446–9. <https://doi.org/10.1007/s11661-017-4428-8>.
- [24] Rokni MR, Nardi AT, Champagne VK, Nutt SR. Effects of Preprocessing on Multi-Direction Properties of Aluminum Alloy Cold-Spray Deposits. *J Therm Spray Technol* 2018;27(5):818–26. <https://doi.org/10.1007/s11666-018-0723-1>.
- [25] Walde C, Cote D, Champagne V, Sisson R. Characterizing the Effect of Thermal Processing on Feedstock Al Alloy Powder for Additive Manufacturing Applications. *J Mater Eng Perform* 2019;28(2):601–10.
- [26] Rokni MR, Zarei-Hanaki A, Abedi HR. Microstructure evolution and mechanical properties of back extruded 7075 aluminum alloy at elevated temperatures. *Mater Sci Eng A* 2012;532:593–600. <https://doi.org/10.1016/j.msea.2011.11.020>.
- [27] Rokni MR, Widener CA, Crawford GA, West MK. An investigation into microstructure and mechanical properties of cold sprayed 7075 Al deposition. *Mater Sci Eng A* 2015;625:19–27. <https://doi.org/10.1016/j.msea.2014.11.059>.
- [28] Liu T, Story WA, Brewer LN. Effect of Heat Treatment on the Al-Cu Feedstock Powders for Cold Spray Deposition. *Metall Mater Trans A Phys Metall Mater Sci* 2019;50(7):3373–87. <https://doi.org/10.1007/s11661-019-05230-z>.
- [29] Barnes J, Champagne V, Ballard D, Eden TJ, Shoffner B, Potter JK, Wolfe DE. AFRL-ML-WP-TP-2007-431 Mechanical and microstructural effects of cold spray aluminum on al 7075 using kinetic metallization and cold spray processes (Preprint), 2007.
- [30] Price TS, Shipway PH, McCartney DG. Effect of Cold Spray Deposition of a Titanium Coating on Fatigue Behavior of a Titanium Alloy. *J Therm Spray Technol* 2006;15(4):507–12.
- [31] Gavras AG, Lados DA, Champagne VK, Warren RJ, Singh D. Small Fatigue Crack Growth Mechanisms and Interfacial Stability in Cold-Spray 6061 Aluminum Alloys and Coatings. *Metall Mater Trans A Phys Metall Mater Sci* 2018;49(12):6509–20. <https://doi.org/10.1007/s11661-018-4929-0>.
- [32] Bagherifard S, Guagliano M. Fatigue performance of cold spray deposits: Coating, repair and additive manufacturing cases. *Int J Fatigue* 2020;139:105744. <https://doi.org/10.1016/j.ijfatigue.2020.105744>.
- [33] White BC, Story WA, Brewer LN, Jordon JB. Fatigue behavior of freestanding AA2024 and AAA7075 cold spray deposits. *Int J Fatigue* 2018;112:355–60. <https://doi.org/10.1016/j.ijfatigue.2018.03.007>.
- [34] Avery DZ, Phillips BJ, Mason CJT, Palermo M, Williams MB, Cleek C, et al. Influence of Grain Refinement and Microstructure on Fatigue Behavior for Solid-State Additively Manufactured Al-Zn-Mg-Cu Alloy. *Metall Mater Trans A Phys Metall Mater Sci* 2020;51(6):2778–95. <https://doi.org/10.1007/s11661-020-05746-9>.
- [35] Anderson TL. Fracture Mechanics: Fundamentals and Applications 2005. <https://doi.org/10.1201/9781315370293>.
- [36] Gavras AG, Lados DA, Champagne VK, Warren RJ. Effects of processing on microstructure evolution and fatigue crack growth mechanisms in cold-spray 6061 aluminum alloy. *Int J Fatigue* 2018;110:49–62. <https://doi.org/10.1016/j.ijfatigue.2018.01.006>.
- [37] Zahiri SH, Fraser D, Gulizia S, Jahedi M. Effect of processing conditions on porosity formation in cold gas dynamic spraying of copper. *J Therm Spray Technol* 2006;15(3):422–30. <https://doi.org/10.1361/105996306X124437>.

- [38] Suresh S, Vasudi~van AK, Bretz PE. Mechanisms of Slow Fatigue Crack Growth in High Strength Aluminum Alloys: Role of Microstructure and Environment, (n.d.).
- [39] Bolotin VV, Babkin AA, Belousov IL. Probabilistic model of early fatigue crack growth. *Probabilistic Eng Mech* 1998;13(3):227–32.
- [40] Todinov MT. A probabilistic method for predicting fatigue life controlled by defects. *Mater Sci Eng A* 1998;255(1-2):117–23.
- [41] Oh J, Kim NJ, Lee S, Lee EW. Correlation of fatigue properties and microstructure in investment cast Ti-6Al-4V welds. *Mater Sci Eng A* 2003;340(1-2):232–42. [https://doi.org/10.1016/S0921-5093\(02\)00176-4](https://doi.org/10.1016/S0921-5093(02)00176-4).
- [42] McDowell DL, Dunne FPE. Microstructure-sensitive computational modeling of fatigue crack formation. *Int J Fatigue* 2010;32(9):1521–42. <https://doi.org/10.1016/j.ijfatigue.2010.01.003>.